Assessing Seismic Damage Through Stochastic Simulation of Ground Shaking: The Case of the 1998 Faial Earthquake (Azores Islands)

G. Zonno · C. S. Oliveira · M. A. Ferreira · G. Musacchio · F. Meroni · F. Mota-de-Sá · F. Neves

Abstract In July 1998, an $M_w = 6.2$ earthquake struck the islands of Faial, Pico and San Jorge (in the Azores Archipelago), registering VIII on the Modified Mercalli Intensity scale and causing major destruction in the northeastern part of Faial. The main shock was located offshore, 8 km North East of the island, and it triggered a seismic sequence that lasted for several weeks. The existing data for this earthquake include both the general tectonic environment of the region and the teleseismic information. This is accompanied by one strong-motion record obtained 15 km from the epicentre, the epicentre location of aftershocks, and a large collection of the damage inflicted to the building stock (as poor rubble masonry, of 2–3 storeys). The present study was carried out in two steps: first, with a finite-fault stochastic simulation method of ground motion at sites throughout the affected islands, for two possible locations of the rupturing fault and for a large number of combinations of rupture mechanisms (as a parametric analysis); secondly, the damage to buildings was modelled using a well-known macroseismic method that considers the building typologies and their associated vulnerabilities. The main intent was to integrate different data (geological, seismological and building features) to produce a scenario model to reproduce and justify the level of damage generated during the Faial earthquake. Finally, through validation of the results provided by these different approaches, we obtained a complete procedure for the parameters of a first model for the production of seismic damage scenarios for the Azores Islands region.

Keywords Stochastic finite-fault scenarios · Building damage assessment · 9th July 1998 Faial earthquake · Azores Islands

G. Zonno (✉) · G. Musacchio · F. Meroni
Istituto Nazionale di Geofísica e Vulcanologia, Sezione di Milano-Pavia,
Via Bassini 15-20133, Milan, Italy
e-mail: zonno@mi.ingv.it

C. S. Oliveira · M. A. Ferreira · F. Mota-de-Sá · F. Neves
Departamento de Engenharia Civil e Arquitectura, Instituto Superior Técnico,
Av. Rovisco Pais, 1049-001 Lisbon, Portugal
e-mail: csoliv@civil.ist.utl.pt

1 Introduction

As a result of its location on the boundary of the triple junction between the three large North American, Eurasian and African tectonic plates, and of a hot-spot (Fig. 1), the Azores Archipelago is subjected to frequent seismic activity. This is also seen by low magnitude seismic sequences triggered occasionally by moderate to large earthquakes. As most of this region is submerged, there is no clear location of the active faults, and the existing data (e.g. geological, geophysical, geodesic and seismological) do not yet fully support a consensus geodynamic model.

During the dawn of 9th July, 1998, an $M_w = 6.2$ earthquake struck the island of Faial, causing major destruction on the northeastern part of the island, where more than 5,000 people were affected. There were eight deaths, 150 people were injured, and 1,500 people were left homeless (Senos et al. 1998). The main shock was located offshore, 8 km North East of the island (Matias et al. 2007), and it triggered a seismic sequence that lasted for several weeks.

This earthquake allowed the collection of an unprecedented quantity of good quality data relating to the damage to constructions. A comprehensive evaluation of this damage and an accurate estimation of the earthquake intensities were provided by a case-by-case analysis of a total of 3,909 damaged buildings, along with damage to monumental structures and to the road network, predominantly near the epicentre. The high level of
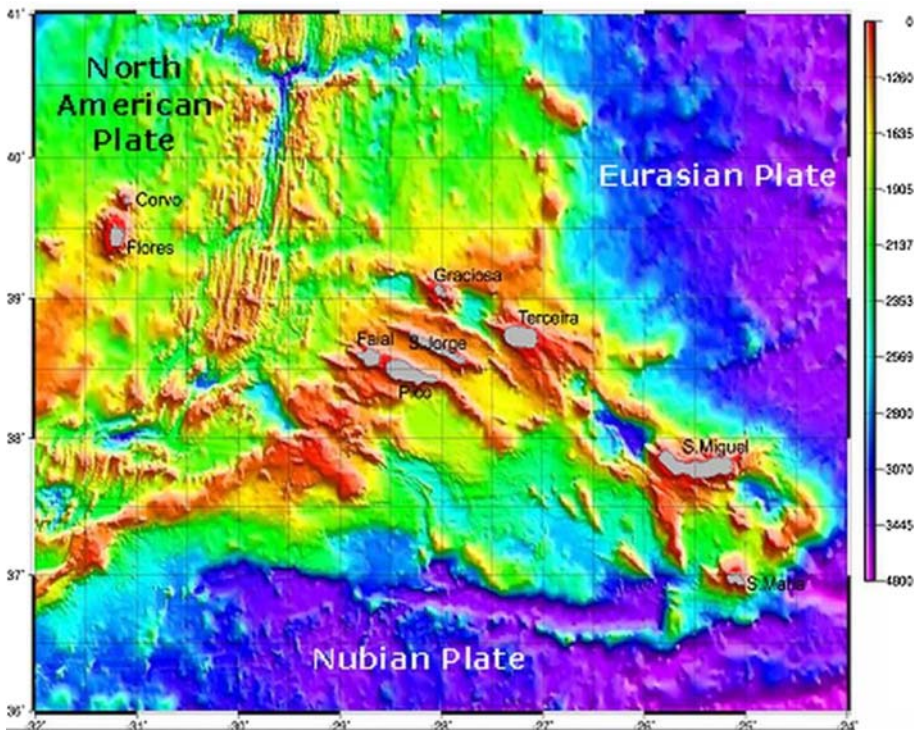

Fig. 1 Colour-coded bathymetry of the Azores plateau. Corvo and Flores Islands (western group); Graciosa, Terceira, Faial and Pico Islands (central group); São Miguel and Santa Maria Islands (eastern group). Redrawn after Lourenço et al. (1998)

destruction revealed by more than 2,100 badly affected buildings located up to 30 km from the epicentre appeared to be related to the high vulnerability of the predominant type of construction-essentially rubble masonry of 2–3 storeys.

The present study is an analysis of the Faial earthquake undertaken for the International Seminar on Seismic Risk and Rehabilitation of Stone Masonry Housing (http://www. azores1998earthquake.org/). The level and variability of earthquake ground-intensity measures depend upon many factors (e.g. Mai 2008), and the techniques of analysis are chosen on the basis of the type, quality and quantity of data available, with a search for the most appropriate approach in relation to the scale of the investigation (e.g. Douglas 2003; Zonno et al. 2009).

Many of the available ground-motion prediction equations were examined in Douglas (2003), in terms of: (1) data selection; (2) accelerogram processing techniques of strong-motion records used to construct the equations; (3) characterisation of an earthquake source; (4) travel path and local site used; and (5) regression techniques used to define the final equations. The ground-motion prediction equations were derived based on different fault-distance metrics, considering magnitude, style of faulting, and various site parameters. However, these equations do not consider finite-fault effects (aside from directivity corrections) and potentially heterogeneous slip distribution effects, or the influence of the relative position of the nucleation point with respect to the overall fault, the areas of large moment release on the fault, and the site location. Indeed, for the Faial earthquake, there was an offshore seismic source very close to the affected islands (Faial and Pico). Hence a finite-fault source was preferred, avoiding the point source approximation of the ground-motion prediction equations (i.e. Spence 2007).

The procedure adopted can be summarised as two steps: (1) use of a stochastic finite-fault method (i.e. the EXSIM software; Motazedian and Atkinson 2005) to furnish a level of shaking in terms of peak ground acceleration (PGA) or spectral acceleration. Calibration of the model parameters was performed with the regional information and using the available strong-motion records as a constraint (see following paragraphs); then (2) selection of a relationship between intensity and shaking parameters, because all available macroseismic data are expressed in the Modified Mercalli Intensity (MMI) scale (Wald et al. 1999). The constraint to evaluate the quality of the relationships available was realised using the macroseismic survey data (Matias et al. 2007). Another comparison at the level of macroseismic intensity was performed with the EMS-98 macroseismic scale obtained from other independent information (Ferreira 2008).

Finally, the damage caused by the Faial earthquake was compared with the "mean damage index" (DI_{mean}) method (Dolce et al. 1999) with the damage obtained through a numerical model using a well-known macroseismic method (Lagomarsino and Giovinazzi 2006). To conclude, the limits and uncertainties of the procedures of analysis used are discussed, and we provide some suggestions regarding the future prospects of improving the procedure itself and its calibration of the area investigated.

2 Tectonic Setting

The Azores plateau marks the boundary between three large plates: the North-American to the West, the Eurasian to the North, and the African to the South (Fig. 1). The 1998 Faial earthquake occurred in the Central Azores Islands, along the Azores-Gibraltar Fault Zone, an oblique spreading centre and a plate boundary with an abnormally thick oceanic crust (Madeira 1998; Lourenço et al. 1998). The NW–SE trending ridges (Vogt 1976; Dias et al.

2007) parallel to the plate boundary occur along a broad sheared region under a trans-tensile stress regime (Fig. 1).

Most of the seismicity and volcanism of these islands are clustered along three strike-slip fault systems that are roughly NW–SE trending and subparallel to the plate boundary (Fig. 2a) (Madeira and Silveira 2003). The fault geometry and kinematics indicate a stress field with the minimum horizontal compressive stress axis (σ_3) trending NE–SW. How-ever, permutations between the maximum (σ_1) and intermediate (σ_2) compressive stress axes (NW–SE horizontal, and vertical, respectively) can originate trans-tensile or tensile regimes (Reches and Dieterich 1983), and can trigger alternating phases of intense tectonic activity and volcanism.

The 1998 Faial earthquake had its epicentre North East of Faial Island (Borges et al. 2007), where seismicity occurs on NNW–SSE-trending strike-slip lineaments, according to the NE–SW trending σ_3. The plane that ruptured in 1998 had an azimuth of 156°, a dip of 85°, and a left-lateral strike-slip motion (Senos et al. 1998).

Shortly after the earthquake, a broad range of locations for the epicentre was issued by the various worldwide networks. This continued even after compilation of large sets of phase readings, due to inaccurate velocity-model and/or location procedures for this par-ticular region of the Earth. Figure 2a shows the dispersion of the epicentre locations provided by different hypotheses, together with the fault plane solution obtained with the Centroid Moment Tensor method (Dziewonski and Woodhouse 1983), as shown in Senos et al. (2008). However, the main shock relocation based on a one-dimensional (1D) velocity model suggested an epicentre about 8 km North East, offshore of Faial Island (EPI 1, Latitude 38.634°N, Longitude 28.523°W), and a hypocentre depth between 2 km and 5 km (Matias et al. 2007).

Seismic tomography analysis demonstrates a plutonic intrusion offshore, between the islands of Faial and Pico (Fig. 2b, c), that is bounded by clusters of seismicity that outline the seismogenic zone (Dias et al. 2007; Schilling 1991; Yang et al. 2006). The 1998 Faial earthquake might have occurred on the western-most flank of the intrusion (EPI 2, Latitude 38.640°N, Longitude 28.590°W; issued by SIVISA). Since high V_P gradients revealed the presence of the fault, while high V_P/V_S ratios translated into rheological changes associated with the slip movement on a fault, it is possible to infer a hypocentre ranging from 4 to 6 km, close to a high-slip patch.

3 Data

3.1 Strong Motion and Surface Geology

The 1998 Faial earthquake was recorded by accelerometric stations located on the Central Azores Islands (Table 1). At the Prince of Mónaco Observatory in Horta town (Faial Island), relatively large ground-shaking was recorded (PGA = 390 mg; see Fig. 3). Fur-ther away, much lower shaking was recorded (PGA = 3–16 mg) in Terceira (GZC, SEB and PVI stations, at 113–133 km) and for the S. Miguel Islands (MOS station, at 250 km). The high value recorded at the Prince of Mónaco Observatory, on the top of a scoria cone in Horta, was due to large local site effects that are seen in time-histories from all of the events recorded there (Escuer et al. 2001). In the nearby downtown area of Horta, the PGA estimated from the behaviour of simple structures (Oliveira et al. 2002) was 200 to 250 mg. These values are more consistent with the light damage suffered by the stock of
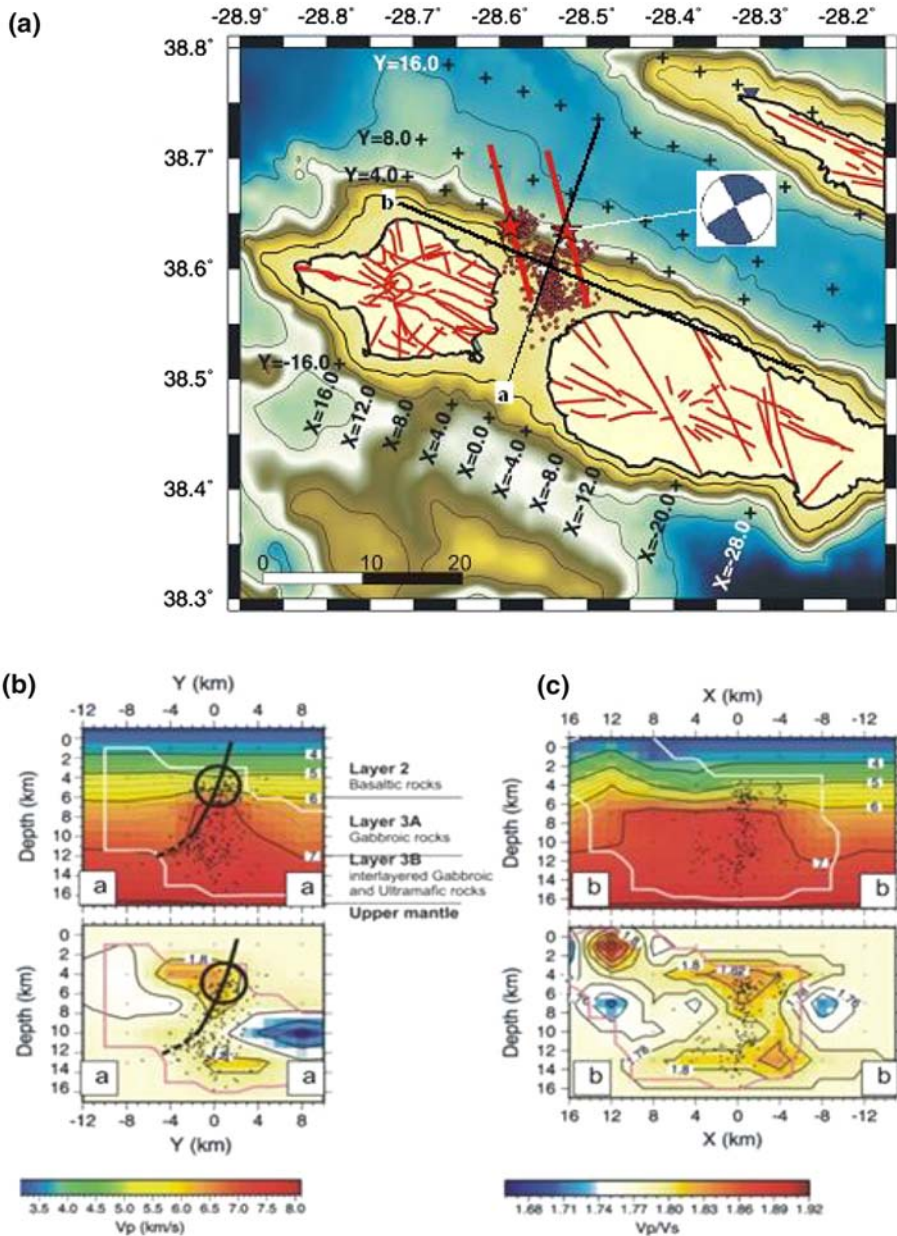
Fig. 2 Tectonic map of the central Azores Islands. **a** Simplified tectonic map of the central Azores Islands (Faial, *left*; Pico, *right*). *Red lines*, faults; *red circles*, epicentres of the seismic sequence triggered by the 1998 Faial earthquake; *red stars*, epicentre locations according to the EPI 1 and EPI 2 (see text) fault-plane solutions (after Senos et al. 2008); *X, Y*, location of the profiles for 3D tomography (Dias et al. 2007); **b, c** Tomographic cross-sections along the line from **a** to **b** on the map. *Top panel*, P-wave velocity colour-coded maps; *bottom panel*, V_p/V_s ratio colour-coded maps

Table 1 Epicentre accelerometric station recordings for the 9th July 1988 Faial earthquake

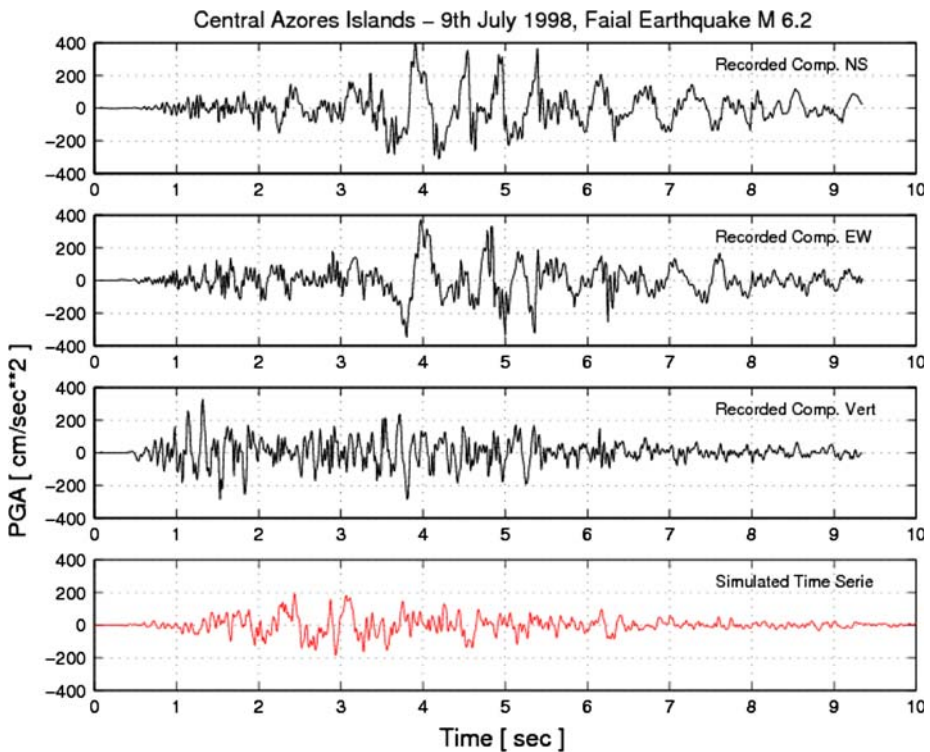| Station code	Lat.	Long.	PGA (mg)	Epicentre EPI 1 Lat. 38.634; Long. −28.523 Distance (km)	Epicentre EPI 2 Lat. 38.640; Long. −28.590 Distance (km)
HORTA (Faial)	38.529	−28.63	~327–400	14.88	12.77
GZC (Terceira)	38.657	−27.22	~12–14	113.25	119.05
SEB (Terceira)	38.668	−27.09	~9–23	124.68	130.47
PVI (Terceira)	38.732	−27.06	~5–10	127.52	133.25
MOS (S. Miguel)	37.890	−25.82	~3–5	248.99	254.68

Fig. 3 Comparison between recorded and simulated records. *Top* three panels (*black lines*): accelerometer time histories recorded at the Horta site (Faial Island). *Bottom* panel (*red line*): horizontal component of an accelerogram computed using EXSIM (average of two). The simulation was carried out with EPI 2 (see Table 1), the model parameters are listed in Table 2, and the automatic random slip distribution was performed with nucleation point 2 (bilateral rupture)

buildings in Horta, with much lower shaking seen in the ground-motion recordings at Terceira and the San Miguel Islands (3–16 mg).

Geological surface formations can change the ground motion observed at the bedrock. The example of the Prince of Mónaco Observatory has been seen in other locations of soft-soil formations, such as in the alluvium valleys in the northeastern part of Faial Island (Oliveira et al. 2002). To better approximate the ground motion at the building foundations, a simplified approach was included to consider the soil influence at such sites;
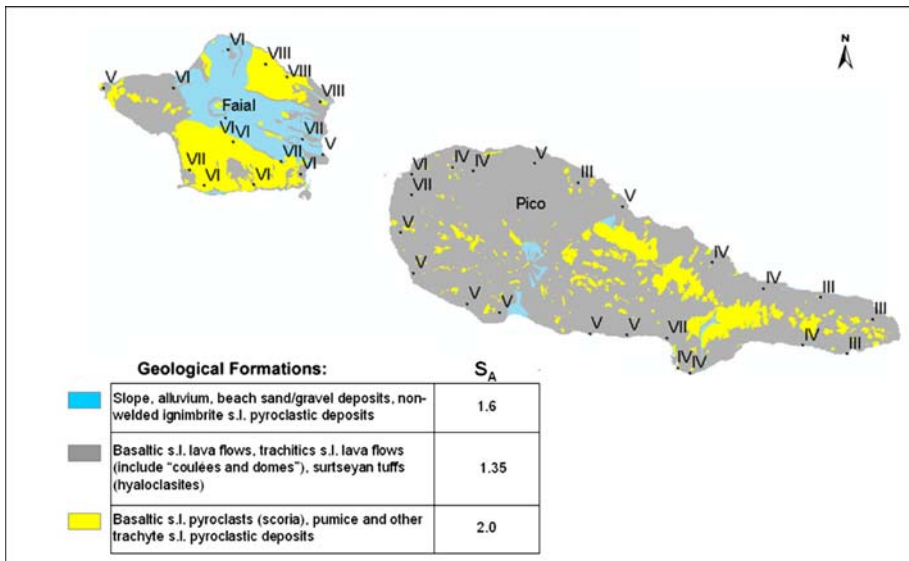
Fig. 4 Lithological map of Faial and Pico Islands, and observed intensities (Modified Mercalli Intensity scale). *Grey*, soft soil formations (type class D—EC8); *blue*, intermediate soil formations (type class C—EC8); *yellow*, hard soil formations (type B—EC8); according to the geotechnical soil classification of the Azores Archipelago (Forjaz et al. 2001). *Source*: Matias et al. (2007)

otherwise, the bedrock input model for damage assessment was too biased, as indicated further below.

Figure 4 shows a large-scale representation of the main superficial geological formations of the Faial and Pico Islands, grouped into three main categories according to Eurocode 8 (EC8 2004). A soil amplification factor (S_A) was assigned to each of these three categories, as proposed in EC8, with values that affected the PGA (see legend to Fig. 4). The S_A values are generally in good agreement with not only the strong-motion records of the Prince of Mónaco Observatory, but also of those other locations where the analytical studies developed support this proposal (Oliveira et al. 2002). The simplified analysis developed herein should be refined in further studies, to provide better estimations of the impact of soil and topographic influences on buildings.

4 Methods

4.1 Stochastic Ground-Shaking Simulation

A finite-fault stochastic method was used to compute the motion with the EXSIM code (Motazedian and Atkinson 2005). As we were interested in sites close to the fault trace, this method overcomes the limitations of the stochastic point-source model. It allows for fault geometry, although the motion from each sub-fault distributed over a fault surface is essentially given by a point-source stochastic simulation. Formally, the motion is computed only at higher frequencies and in the frequency range of engineering interest. The EXSIM finite-fault simulation programme (Motazedian and Atkinson 2005) has been extensively used in the scientific community (Boore 2009; Atkinson et al. 2009) for

purposes similar to that of the present study (e.g. Berardi et al. 2000; Carvalho et al. 2008; Galluzzo et al. 2008; Castro et al. 2008).

The fault plane was assumed to be a rectangle broken into an appropriate number of sub-faults, which are modelled as point sources using the approach of Boore (2003). The sub-faults have ω^2 spectra, and their sizes define the moment and corner frequency, while the number of triggered sub-faults is adjusted to reach a specified target moment. As merely kinematics, the finite-fault approach can provide simulations in good agreement with observations over much of the frequency range of engineering interest (e.g. Hartzell et al. 1999; Motazedian and Atkinson 2005).

The finite-fault model parameters require specification of: (1) the fault-plane geometry (length, width, orientation); (2) the source (slip distribution, stress drop, nucleation point, rupture velocity); and (3) the crustal properties of the region (e.g. geometric spreading coefficient, quality factor $Q(f)$). The ground motion at the bedrock was computed for two possible epicentre locations, EPI 1 and EPI 2 (Table 1), while neglecting the site-specific soil responses. Source scaling relationships (Wells and Coppersmith 1994) provided a fault-plane dimension of 16.5-km length and 9.4-km width for an $M_w = 6.2$ event, while the aftershock distribution, the focal plane solution (Senos et al. 2008.), and tomographic studies (Fig. 2) suggested a 165° strike and an 85° dip. The fault dimensions were consistent with the plate structure derived by seismic tomography, and with an aftershock distribution that showed a brittle plate within 4 and 14 km of depth at the hypocentral location (Fig. 2).

The number of sub-faults (nine along the length, and five across the width) were set to have almost square dimensions, while the depth at the upper edge of 1.1 km was derived from published seismological studies (Matias et al. 2007; Dias et al. 2007). The shear-wave velocity and density were inferred by combining petrological interpretations of seismic tomography inversions (Matias et al. 2007; Dias et al. 2007) with published data on elastic properties of oceanic crustal rocks (Carmichael 1990, and references therein). The stochastic waveform computation only requires crustal averages of S-wave velocity and density, while P-wave velocities are not specified. Simple assumptions based on the tomographic P-wave velocity (Fig. 2b, c; Table 2) were used to derive the average shear-wave velocity and density for the entire crust. The number of recordings was not large enough to allow highly constrained ground-shaking analyses, as in the near-field only one was obtained for the accelerogram of the 1998 Faial earthquake. The other records were too far away to constrain the solution in the near-field. Therefore, at Faial Island, where the damage was assessed, some of the parameters used in the stochastic modelling had to be defined by making simple assumptions and using the available published information.

The source-model parameters were defined assuming two different slip models (automatic random, Gaussian distribution) computed on given nucleation points for a moment magnitude of $M_w = 6.2$, a stress drop of 200 bars, and a rupture velocity on the fault of 0.8-fold the shear-wave velocity (Table 2). This stress drop of 200 bars was consistent with that derived from P-wave spectral analysis (Borges et al. 2007), and with a 200-bar deviatoric stress at 5 km in depth (Matias et al. 2007).

As the geometrical spreading coefficient and the quality factor, Q(f), are crucial to ground-shaking simulation, and due to the lack of attenuation information specific for the studied area, a value was assumed from that used in areas with similar geodynamic settings (Ólafsson et al. 1998; Carvalho et al. 2008).

The distance-dependent duration (To + 0.1 R, with To = 4.0) was selected according to other previous simulation studies and validated with the average duration of the horizontal components at the Horta station. The duration chosen at the Horta station is

Table 2 Finite-fault ground-shaking simulation parameters

Parameter	Value
Moment magnitude	6.2
Fault orientation	Strike 165°, dip 85°
Depth of top	1.1 km
Fault dimensions	Length (width) 16.5 (9.4) km
Number of sub-faults	Along length 9, along width 5
Fast Fourier Transform	16,384 points
Sample interval	0.005 s
Shear-wave velocity	3.5 km/s
Density	2.8 g/cm^3
Rupture velocity	$0.8 \times$ shear wave velocity
K	0.03 s
$Q(f)$	$239.0 * f^{1.06}$
Stress drop	200 bar
Geometric attenuation	If $R < 30$, R^{-1}; else $R^{-0.5}$
Distance-dependent duration	To + 0.1 R (s)
Windowing function	Saragoni-Hart
Amplification function	Not applied
Slip model	Random and Gaussian
Dynamic flag and pulsing (%)	1 and 50.0
Damping	5% critical damping

consistent with the observed duration on the horizontal component waveforms (Fig. 3). The computed motion is not a full wave field, with only S-waves simulated, and the resulting waveforms are averaged between the two horizontal components (Fig. 3). Among the computed ground-shaking parameters, PGA (cm/s^2) and response acceleration spectra (PSA; cm/s^2) were used, considering 20 runs of the stochastic process.

The intensity of the ground shaking can be inferred through empirical relationships between the recorded PGA, PGV and MMI developed from observations in several areas of the World (Wald et al. 1999; Bootwright et al. 2001; Atkinson and Kaka 2007). However, recent studies have suggested that these MMI relationships are strongly dependent on efficient propagation of high-frequency radiation and/or occurrence of thick sediment embayments (Atkinson and Kaka 2007). We tested the relationship of Wald et al. (1999) as it is the most widely used, which computes the MMI as a function of PGA and PGV. The relationships are written as follows:

$$MMI = 3.66 \log(PGA) - 1.66 \quad \text{if} \quad V \leq MMI \leq VIII \quad (\sigma = 1.08) \tag{1}$$

$$MMI = 3.47 \log(PGV) + 2.35 \quad \text{if} \quad V \leq MMI \leq IX \quad (\sigma = 0.98) \tag{2}$$

In Equation (2), the PGV was derived with the approximate relationship suggested by Bommer and Alarcon (2006):

$$PGV(cm/s) = PSA_{(0.5s)} / 20 (cm/s^2) \tag{3}$$

Although Wald et al. (1999) suggest that high intensities correlate better with PGV than PGA, Equation (2) was inadequate for our study areas. One reason for this appears related to the approximation used to derive PGV (Equation (3)), although this is widely used in the
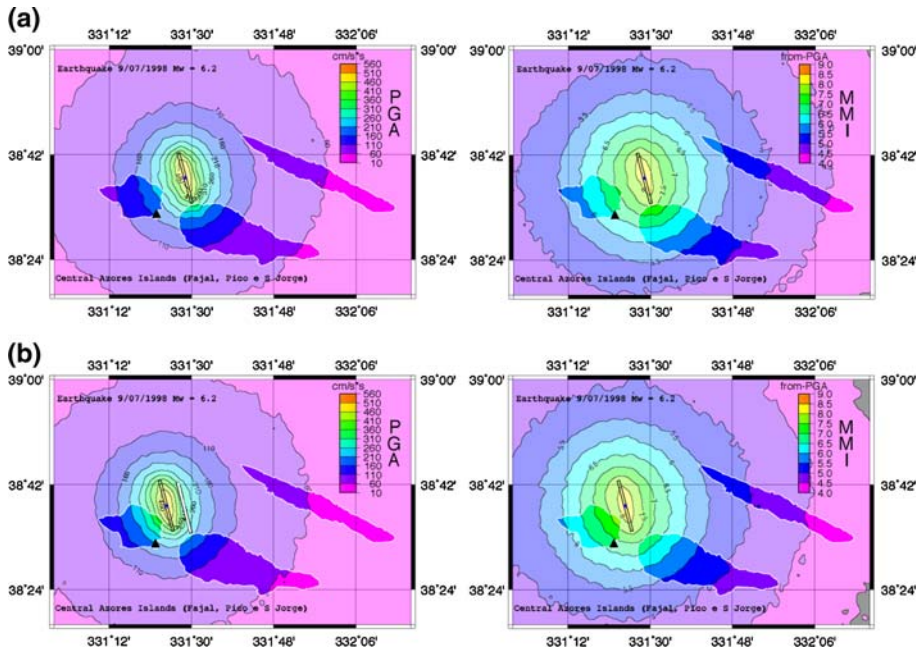
Fig. 5 PGA and MMI maps for the central Azores Islands (Faial, Pico and S. Jorge). The maps were computed on a 0.02° × 0.02° grid using EXSIM, and the parameters are listed in Table 2. **a** Maps using EPI 1, and the location of EPI 1; **b** Maps using EPI 2, with the location of EPI 1 shown for comparison. Intensity was computed from the PGA (cm/s²) using Relationship (1) (Wald et al. 1999). *Black triangle*, the Horta site on Faial Island

engineering community. Simulated intensities of ground shaking are more consistent with the observed intensities if Equation (1) is used.

Two ground-shaking scenarios were considered using the two epicentres discussed above, and the PGA and MMI maps were constructed (Fig. 5), with the MMI values compared using field data (Matias et al. 2007) and the ground-motion simulation for Faial Island. Isoseismic maps were drawn using the ArcGIS interpolation Inverse Distance Weight (IDW) method (Watson and Philip 1985).

Depending on the epicentre location, the resulting higher levels of ground shaking shifted 2 km in the East–West direction. Since a westward shift of high values of MMI is more consistent with the field data, from here on only EPI 2 was used to retrieve seismic damage. Figure 10 shows the macroseismic intensity distribution of the Faial earthquake as expressed through the MMI intensity scale. The left panel is based on the field observations (Matias et al. 2007), and in the panels from the middle to the right, the intensity values are computed according to a fault-rupture model. This uses the different hypotheses of epicentre locations (EPI 1 and EPI 2), and does not including the soil influences, because regional terms were being considered. The maximum intensity observed in Faial is VIII on the MMI scale (Fig. 4); however, given the high level of destruction seen in some localities, this indicates that the intensities at individual sites might have been one grade higher than those of the regional values plotted on the maps, as also seen if the soil influence is included.

4.2 Parametric Analysis

A parametric analysis of the finite-fault bedrock stochastic simulation at the Horta site was performed to estimate the range of variations in amplitude and frequency. Our set of simulations are based on simplified sources with uniform slip, uniform rise times, and a constant rupture speed. They are aimed at obtaining rough first-order estimations of the influence of some of the key parameters, while keeping the slip distribution and nucleation point fixed. These estimations include the slip models (Fig. 6) and hypocentre position, as well as the $Q(f)$ and stress drop.

Slip models are generated assuming a Gaussian distribution centred on nucleation points NP 1, NP 2 and NP 3, and NP 4 (Fig. 6), or using a random slip distribution generated automatically by EXSIM. On each slip model, four hypocentre positions have been set (nucleation points) located: (1) in the lower half of the fault, left-hand side; (2) in the lower half of the fault, right-hand side; (3) in the centre of the fault; and (4) randomly. Therefore, the final values were obtained from 16 rupture models (four hypocentres and four slip distributions); at the Horta site, these resulted in 480 stochastic time series, and 120 time series for each slip model.

The resulting ground-shaking scenarios are also considered in terms of the PGA of the 30 stochastic realisations, compared with the observed acceleration-time history, to determine the best agreement to the PGA recorded (Fig. 7). The medians, 75th and 84th percentiles, means, modes, minima and maxima considering the PGA are calculated for each of the time series of the 30 stochastic realisations. The highest PGA is for the SLIP 3 slip distribution and the centred nucleation point (time series HORTA 01-28-32.acc in Fig. 7). However, waveforms can look very different for both amplitude and frequency content depending on the chosen slip distribution and the position of the hypocentre on the fault plane that controls the rupture directivity. If the simulated (Fig. 7, EW) and observed time histories at the Horta site are compared, this provides a qualitative estimate of site effects that influences the ground-motion variability. Although the 75th percentile time series best resembles the observed EW waveform, the maximum must be considered from among the simulated PGAs to have the closest match with the observed value.

Another way to highlight the statistics-derived PGAs is by comparing the frequencies of the PGA classes for all of the rupture models (Fig. 8, yellow bars) with those derived for
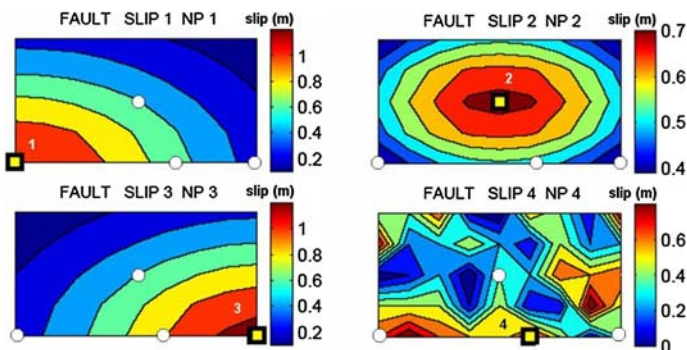

Fig. 6 Colour-coded slip distributions used in the parametric study at the Horta site. The nucleation points are plotted on each slip map (Slip 1, Slip 2, Slip 3 and Slip 4): bold black squares and numbers, nucleation points centred on highest slip patch; white circles, other nucleation points. Bottom right panel: random slip distribution generated by EXSIM, using the parameters listed in Table 2
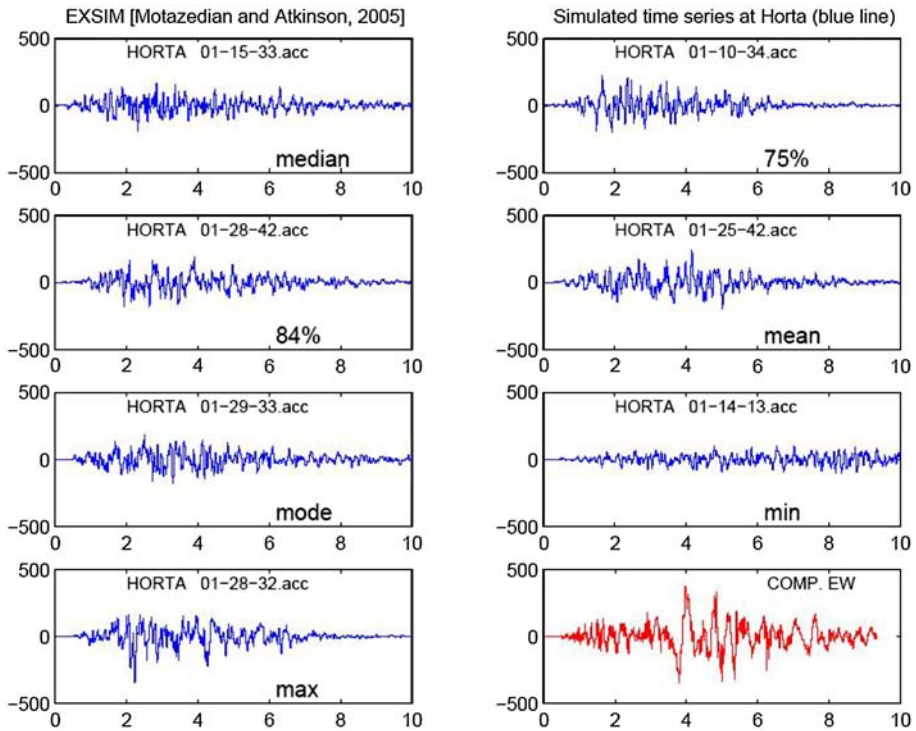
Fig. 7 Simulated time series. Simulated time series derived for the median, 75th (75%) and 84th (84%) percentiles, mean, mode, minimum and maximum PGA (cm/sec^2). Each time series represents the one (among all of the 480 time series) that is closest to these absolute values. *Red*, recorded E–W component waveform at the Horta site

each of the four models (SLIP 1–3, random). The slip distribution of SLIP 3 reveals a trend in frequency *versus* PGA class (Fig. 8, green bars) that is shifted to a higher class of PGA. We can plot the response spectra of only the time series that have the maximum PGAs among the 30 stochastic realisations, and compare these to the observed data at the Horta site (Fig. 9). Useful information can be extracted from the response-acceleration spectrum despite the lack of observed data as, for instance, the observed PSA represents the upper limit of the simulated one. Moreover, since the model does not generate low frequency waveforms, we cannot consider the PSA in its low frequency range (1–3 Hz). No matter which rupture model is used, it is not possible to exactly match the observed PSA in the 30–40 Hz frequency range. This might be related to site and/or directivity effects on the wave propagation (Fig. 10).

5 Seismic Damage Assessment

5.1 Building-Stock Characterisation and Post-Earthquake Damage Assessment

The traditional architecture of the islands is a simplicity of construction based on the use of rubble-stone masonry, wooden floors and roof. This gives the Azorean constructions the
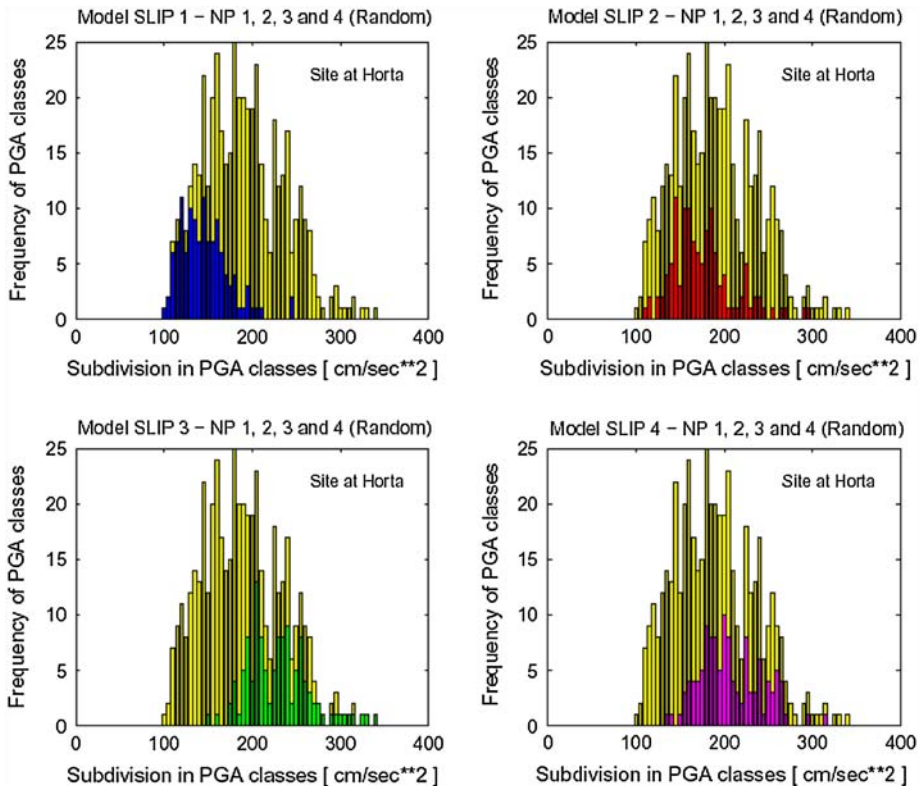
Fig. 8 Frequency of PGA classes versus PGA for the four slip models. *Yellow bars*, EPI 2; *blue bars*, SLIP 1; *red bars*, SLIP 2; *green bars*, SLIP 3; *magenta bars*, SLIP 4

right to be considered a heritage of humanity, for their richness and formal variety in the combination of the different construction elements that make up these buildings. Normally, following an earthquake, some types of repairs produce changes to the traditional construction systems, techniques and materials. This arises from the poor seismic response that some buildings show, which is often associated with a lack of maintenance or with damage that was suffered in previous earthquakes. This will interfere with the traditional buildings, so to understand the structural behaviour of the constructions, it is of extreme importance to know the types of changes that have been introduced into the building stock and to characterise the traditional construction that was maintained following the earthquake.

The most widely used type of construction in the central Azores Islands are "traditional construction" and "altered traditional construction" (Fig. 11; Table 3: TC, ATC, respectively), which are highly vulnerable structures that were severely damaged during the earthquake.

As cited above, locations and characteristics of buildings were obtained from a survey conducted after the earthquake. These were further updated in 2007, and a database was developed to facilitate rapid analyses. After a careful analysis of the 3,909 buildings in the database from the parishes of Faial and Pico, Ferreira (2008) classified the building damage according to the 1998 European Macroseismic Scale (EMS-98) (Grunthal 1998). The EMS-98 scale provides the possibility of dealing with these different types of buildings,
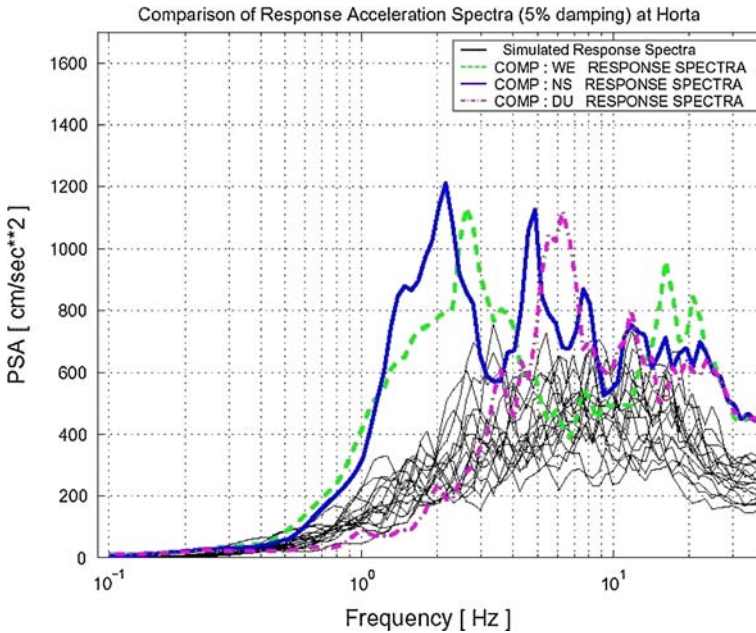
Fig. 9 Comparison of the response acceleration spectra at Horta. Acceleration spectra (5% damping) at Horta station for the horizontal components. Recorded responses: *blue*, NS; *green*, WE; *magenta*, DU. Simulated response: *black*

Fig. 10 Colour coded MMI scale intensity maps. *Left* to *right*: MMI map derived from the surveyed data; MMI map computed from the PGA (Wald et al. 1999) using EPI 1; MMI map computed using EPI 2. The isoseismal maps were drawn using the ArcGIS interpolation Inverse Distance Weight (IDW) method

including five possible degrees of damage that are related to the level of structural and non-structural damage to an entire building (D1—negligible-to-slight damage; to D5—total destruction).

This post-earthquake damage database contains numeric data to quantify the percentage of damage to walls (exterior and interior), floors and the roof, and sometimes contains photographs of the houses, as well as a field for the "description of damage". Unfortunately, detailed descriptions of these parameters are not always available; sometimes there are only comments or general notes about the situation of the owners and tenants available, along with other information that is not relevant to the present study. This assessment also provided damage grades for 2,030 buildings in Faial and 885 in Pico; out of these, 1,468 were geo-referenced in Faial and 559 in Pico. This allowed the development of geospatial analyses to determine, for instance, the distribution of buildings with a given damage grade
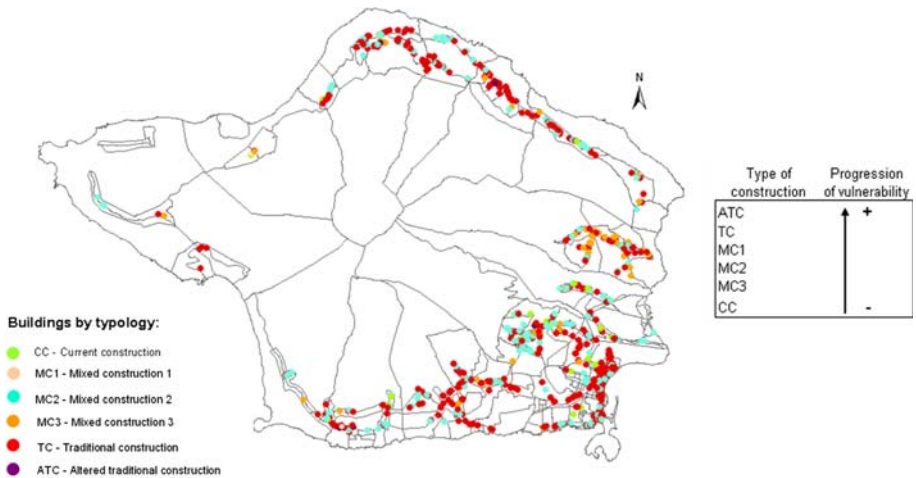
Fig. 11 Distribution of building types on Faial Island. Main panel: colour-coded spatial building distribution by construction class. *Right* panel: relationships between construction classes and vulnerability

Table 3 : Descriptions of the common structural systems of Faial and Pico Islands

Construction class	Description
TC	"Traditional construction"—the structure is mainly stone masonry, with wooden floors and roof
ATC	"Altered traditional construction"—very similar to traditional construction (structure in stone masonry and wooden roof), but parts of the floors (often bathroom and kitchen) are made of reinforced concrete
MC1	"Mixed construction 1"—structure is masonry stone, with concrete floors and wooden roof
MC2	"Mixed construction 2"—structure is masonry stone, but there are reinforced concrete columns and beams, wooden floors, wooden roof and concrete enlargements
MC3	"Mixed construction 3"—reinforced concrete columns, beams and floors, either wooden or concrete roof
CC	"Current construction"—earthquake-resistant structures, where almost all elements of the house are reinforced concrete, except for the roof, which can be of wood

throughout a given area (Fig. 12). The inland faults, landslides and individual buildings superimposed on the same map have provided a better understanding of the damage grades to the buildings, indicating the damage that resulted from the earthquake.

5.2 Seismic Damage Using the Mean Damage Index

Another way to assess this damage is through the DI_{mean} (Dolce et al. 1999), extended to a larger geographical unit (parish/"freguesia"):

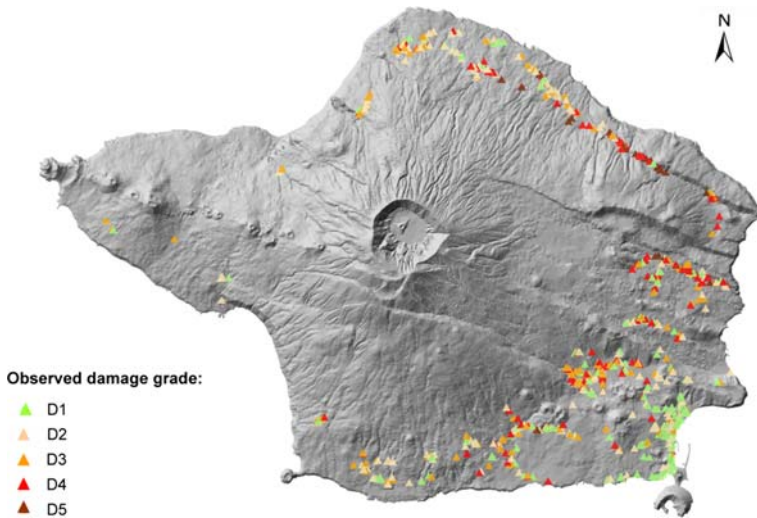$$DI_{mean} = \sum_{i=1}^{5} \frac{d_i f_i}{n} \tag{4}$$

Fig. 12 Observed damage grades. Damage grade classification using the EMS-98 scale directly from the observed data (Ferreira 2008). D1, negligible to slight damage; D2, moderate damage; D3, substantial to heavy damage; D4, very heavy damage; D5, total destruction

where d_i is the normalised damage grade ($d_i = 1,...5$, not-null damage levels, $n = 5$), and f_i is the relevant frequency within the geographical unit. DI_{mean} ranges from 0 to 1; where $DI_{mean} = 0$ indicates a total absence of damage, and $DI_{mean} = 1$ is for total destruction.

This DI_{mean} (0–1 scale) is a synthetic tool to account for the expected damage. As seen in Fig. 13, for each census tract ("freguesia"), a DI_{mean} was derived and, in particular, the analysis shows the presence of three census tracts (Salão, Ribeirinha and Pedro Miguel), with $DI_{mean} = 0.60$–0.80. These correspond to the parish with the most vulnerable buildings and the highest level of destruction (partial and total collapse). This approach shows an overall pattern similar to the intensity map shown in Fig. 10 (left), and proves that the building-by-building damage evaluation described in this section is a good indicator of the macroseismic intensities obtained in the field.

5.3 Seismic Damage Using the Macroseismic Method

To simulate damage scenarios, the ground motion and the seismic vulnerability of the building stock are needed. In the macroseismic EMS-98 scale, five discrete damage grades can be selected (D1 to D5) to describe the damage grades of the main structural components and non-structural elements. The Lagomarsino and Giovinazzi approach was obtained by analysing how the EMS-98 macroseismic scale suggests implicit and fuzzy values for the probability damage matrix for the different classes of buildings, as opposed to the standard procedure of estimating the local macroseismic intensities on the basis of damage observed. Therefore, they "transposed" the linguistic expression of the vulnerability matrix given by EMS-98 for each vulnerability class of building into numerical bounds of the probability of any damage level. Following this method, once a value has been fixed for building vulnerability (V_I) and intensity I, a mean damage grade (μ_D) can be determined using the following analytical function (proposed in Giovinazzi and Lagomarsino (2003), Lagomarsino and Giovinazzi (2006) and Bernardini et al. (2007)):
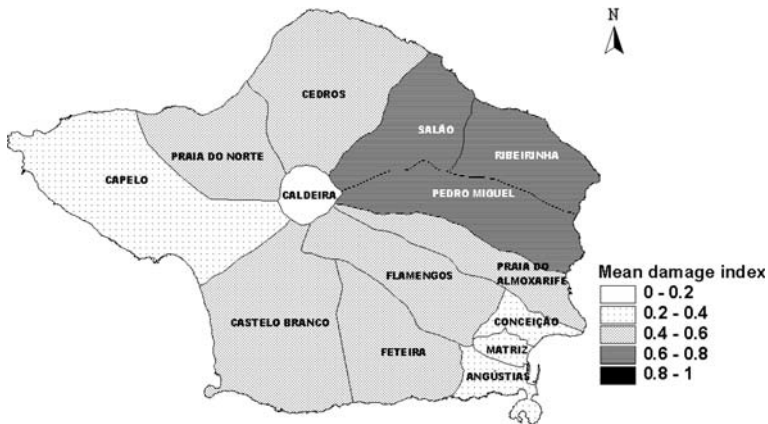
Fig. 13 Mean damage index map for Faial Island for each census tract. Analysis of Faial Island subdivided into census tracts ("freguesia") using the DI_{mean} method (Dolce et al. 1999), showing, in particular, the census tracts with the highest levels of damage (Salão, Ribeirinha and Pedro Miguel)

$$\mu_D = 2.5 + 3 \tanh\left(\frac{I + 6.25 V_I - 12.7}{3}\right) \times f(V_I, I) \tag{5}$$

where $f(V_I, I)$ is defined as:

$$f(V_I, I) = \left\{ \begin{array}{ll} e^{\left(\frac{V_I}{2} \times (I-7)\right)}, & I \leq 7 \\ 1, & I > 7 \end{array} \right\} \tag{6}$$

5.4 Application to Faial Island

Two models of ground motion were used, based on fault rupture EPI 2 for each of the 1,669 buildings for which damage assessment was available (D1–D5). The first model (M-I) considers bedrock intensities, while the second model (M-II) considers the influence of the soil through the simplified amplification factor (S_A). The mean damage grades (μ_D) obtained with M-I and M-II were compared building by building with the observed damage of Fig. 12.

Statistical analyses of the differences between *observed* and *estimated* damage grades were performed using the Minitab 15.1® statistical software (2006). Even though the differences are important in several cases, for model M-I (Fig. 14a) the mean value of the differences is almost one degree (0.9438) (damage grade), with a 95% confidence interval of 0.87 to 1.01; for M-II (Fig. 14b), this error is almost zero (0.0367), with a 95% confidence interval of -0.03 to 0.11.

Taking M-II as a better solution, comparison can be made between the observed and estimated damage grades (grade by grade; Fig. 15). Even though the overall averages are similar, for damage grade D2–D3, M-II overestimates the observed damage, while slightly underestimating it for D1 and D4–D5. The discrepancies between the simulated levels of damage (Fig. 13) and the observed damage (Fig. 12) arise from the uncertainties in the use of this procedure, as specified as follows:

(a)   The simplified model for the surface geology, which requires further refinement;
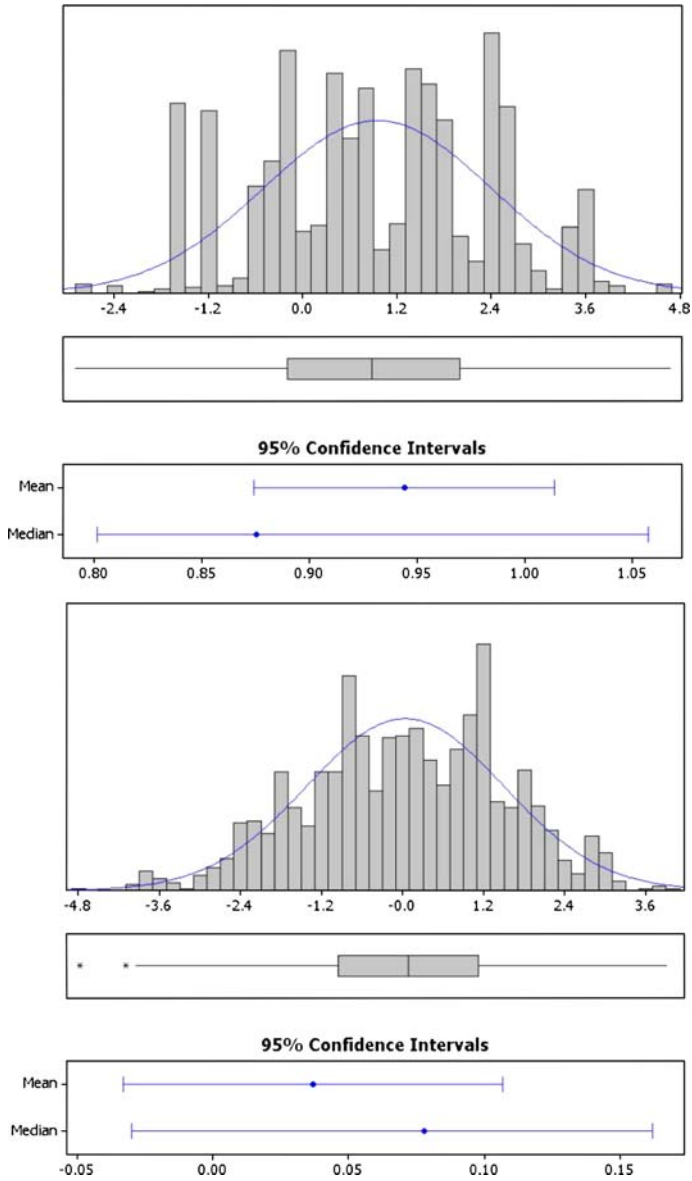(b)   The conversion of PGAs into EMS-98 intensities, which might exceed one degree;

Fig. 14 Summary of statistical analysis of the differences between the observed and estimated damage using the models. Estimated damage according to M-I (**a**) and M-II (**b**) (see text)

(c) The classification of the typologies of the rubble-stone masonry structures into EMS-98 categories;

(d) The uncertainties involved in the Lagomarsino and Giovinazzi method, which might account for another degree of damage (only mean value estimators have been used).
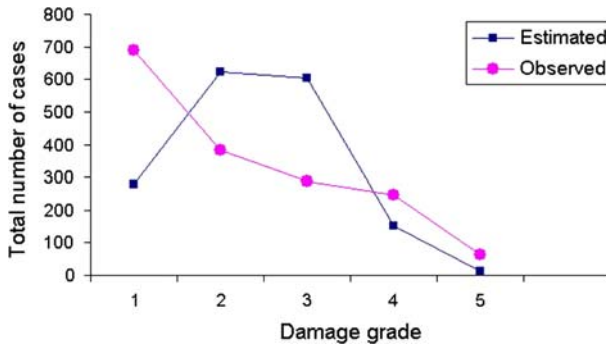
Fig. 15 Observed and estimated damage obtained with the M-II model

If the estimations from the individual buildings are averaged out as parishes, the results from these simulations would be more closely related to the reality as the heavy and low damage average out.

6 Discussion and Conclusions

Finite-fault ground-shaking stochastic simulation allows parameters to be retrieved as the input for assessment of seismic damage. However, the method computes ground shaking at the bedrock without taking into account the influence of site effects that soft soil might have on the final shaking. This could be the case for the high levels of shaking that were recorded at the Horta station. To better reproduce the amplitude and frequency contents of the recorded ground motion at the Horta station, more geological and geotechnical site information will be introduced into future analyses. To investigate the high levels of PSA at low frequencies (see Fig. 9), full-wavefield finite-fault simulations (e.g. the COMPSYN software; Spudich and Xu 2003) will probably be necessary to produce better results at the Horta station for low frequencies ($f < 3$ Hz).

On the basis of the tectonic environment and the most recent interpretations of possible fault mechanisms, a large set of ground-motion simulations have been developed that consider the various rupturing hypotheses (a parametric analysis). Despite the limits of our analysis in terms of the input-model parameters, it has been possible to conclude that in terms of MMI shaking, the EPI 2 scenario parameter best reproduced the observed effects of the Faial Earthquake.

The seismic damage scenarios computed from the DI_{mean} allow the inference that high values of this index ($DI_{mean} = 0.6$–0.8) correspond to the most vulnerable buildings according to the EMS-98 scale. By introducing a simple soil characterisation of the site based only on three classes, it was possible to reproduce the mean damage observed. A more refined analysis of the soil model with more details of the vulnerability classification and the choice of other estimators of shaking parameters (e.g. mode, median, maximum, 75th percentile) should provide better results for reproduction of the damage effects.

A future improvement to this seismic damage procedure would include a calibration of a probabilistic relationship combining EXSIM macroseismic simulations with EMS-98 surveys based not only on the Fail Earthquake information, but also on other events that have occurred in the Azores Islands region.

References

Atkinson GM, Kaka SI (2007) Relationships between felt intensity and instrumental ground motion in the Central United States and California. Bull Seismol Soc Am 97–2:497–510

Atkinson GM, Boore DM, Assatourians K, Campbell K, Motazedian D (2009) A guide to differences between point source and finite fault simulations. Bull Seism Soc Am 100 (in press)

Berardi R, Jiménez MJ, Zonno G, García-Fernández M (2000) Calibration of stochastic finite fault ground motion simulations for the 1997 Umbria-Marche, central Italy, earthquake sequence. Soil Dynamics and Earthquake Engineering 20:315–324

Bernardini A, Giovinazzi S, Lagomarsino S, Parosi S (2007) The vulnerability assessment of current buildings by a macroseismic approach derived from the ems-98 scale. 3° Congreso Nacional de Ingeniería Sísmica. Girona, 8–11 Mayo 2007, Spain

Bommer JJ, Alarcon JE (2006) The prediction and use of peak ground velocity. Journal of Earthquake Engineering 10(1):1–31

Boore DM (2003) Simulation of ground motion using the stochastic method. Pure Appl Geophys 160:635–676

Boore DM (2009) Comparing stochastic point- and finite-source ground-motion simulations: SMSIM and EXSIM. Bull Seism Soc Am 100 (in press)

Bootwright J, Thywissen K, Seekins L (2001) Correlation of ground motion and intensity for the 17 January 1994 Northridge, California earthquake. Bull Seism Soc Am 91:739–752

Borges JF, Bezzeghoud M, Buforn E, Pro C, Fitas A (2007) The 1980, 1997 and 1998 Azores earthquakes and some seismo-tectonic implications. Tectonophysics 435:37–54

Carmichael SR (1990) Practical handbook of physical properties of rocks and minerals. CRC Press, USA, p 741

Carvalho A, Zonno G, Franceschina G, Serra Bilé J, Campos Costa A (2008) Earthquake shaking scenarios for the metropolitan area of Lisbon. Soil Dynamics and Earthquake Engineering 28:347–364

Castro RR, Pacor F, Franceschina G, Bindi D, Zonno G, Luzi L (2008) Stochastic strong-motion simulation of the Mw 6 Umbria-Marche earthquake of September 1997: comparison of different approaches. Bull Seism Soc Am 98(2):662–670

Dias NA, Matias L, Lourenço N, Madeira J, Carrilho F, Gaspar JL (2007) Crustal seismic velocity structure near Faial and Pico Islands (AZORES), from local earthquake tomography. Tectonophysics 445:301–317

Dolce M, Goretti A, Masi A (1999) Analisi dei danni causati dal sisma del settembre 1998 nel Pollino. Ingegneria Sismica, Anno XVI–N 3:5–15

Douglas J (2003) Earthquake ground-motion estimation using strong motion records: a review of equations for the estimation of peak ground acceleration and response spectral ordinates. Earth Sci Rev 61:43–104

Dziewonski AM, Woodhouse JH (1983) Studies of the seismic source using normal-mode theory. In: Kanamori H, Boschi E (eds) Earthquakes: observation, theory, and interpretation: notes from the international school of physics "Enrico Fermi" (1982: Varenna, Italy). North-Holland Publ. Co, Amsterdam, pp 45–137

Escuer M, Oliveira CS, Dessai P, Lopes H (2001) Study of the amplification of seismic waves in Monte das Moças, Horta. Confrontation of records obtained at the seismographic and accelerographic stations. Proceedings 2° Simpósio de Meteorologia e Geofísica da APMG, 3° Encontro Luso-Espanhol de Meteorologia. Évora, Portugal, 105–109

Eurocode 8 (2004) Design of structures for earthquake resistance-part 1: general rules, seismic actions and rules for buildings. EN 1998-1:2004; Comité Europeéen de Normalisation, 224

Ferreira MA (2008) Classificação dos danos no edificado com base na EMS-98. Sismo 1998—Açores. Uma década depois. In Oliveira CS, Costa A, Nunes JC (eds) Governo dos Açores/SPRHI, S.A., 501–512

Forjaz VH, Nunes JC, Guedes JHC, Oliveira CS (2001) Classificação geotécnica dos solos vulcânicos dos Açores: uma proposta. Associação Portuguesa de Meteorologia e Geofísica (ed) Proceedings II Simpósio de Meteorologia e Geofísica—Comunicações de Geofísica, Évora, Portugal, 76–81

Galluzzo D, Zonno G, Del Pezzo E (2008) Stochastic finite-fault ground-motion simulation in a wave-field diffusive regime: case study of the Mt. Vesuvius Volcanic Area. Bull Seism Soc Am 98(3):1272–1288

Giovinazzi S, Lagomarsino S (2003) Seismic risk analysis: a method for the vulnerability assessment of built-up areas. Proceedings European Safety & Reliability Conference, Maastricht, 16

Grunthal G (1998) European Macroseismic Scale 1998. Cahiers du Centre Eur de Géodyn et de Séismologie 15:1–99

Hartzell S, Harmsen S, Frankel A, Larsen S (1999) Calculation of broadband time histories of ground motion: comparison of methods and validation using strong-ground motion from the 1994 Northridge earthquake. Bull Seismol Soc Am 89:1484–1504

Lagomarsino S, Giovinazzi S (2006) Macroseismic and mechanical models for the vulnerability and damage assessment of current buildings. Bull Earthquake Eng 4:415–443

Lourenço N, Miranda JM, Luís JF, Ribeiro A, Mendes-Victor LA, Madeira J, Needham HD (1998) Morpho-tectonic analysis of the Azores Volcanic Plateau from a new bathymetric compilation of the area. Marine Geophys Res 20(3):141–156

Madeira J (1998) Estudos de neotectónica nas ilhas do Faial, Pico e S. Jorge: Uma contribuição para o conhecimento geodinâmico da Junção Tripla dos Açores. Ph.D. Thesis, Universidade de Lisboa, Lisboa (3), 537–546

Madeira J, Silveira AB (2003) Active tectonics and first paleoseismological results in Faial, Pico and S. Jorge islands (Azores, Portugal). Annals of Geophysics 46(5):733–761

Madeira J, Silveira AB, Serralheiro A (1998) Efeitos geológicos do sismo do Faial de 9 de Julho de 1998. Protecção Civil (Revista do Serviço Nacional de Protecção Civil) 14:12–20

Mai PM (2008) Ground motion: complexity and scaling in the near field of earthquake ruptures. In: Lee WHK, Meyers R (eds) Encyclopedia of complexity and systems science. Springer, Berlin

Matias L, Dias NA, Morais A, Vales D, Carrilho F, Gaspar JL, Senos L, Silveira AB (2007) The 9th July 1998 Faial Island (Azores, North Atlantic) seismic sequence. J Seismology 11:275–298

Minitab 15.1® (2006) Minitab statistical software. Minitab Inc

Motazedian D, Atkinson GM (2005) Stochastic finite-fault modelling based on a dynamic corner frequency. Bull Seismol Soc Am 95(3):995–1010

Ólafsson S, Sigbjörnsson R, Einarsson P (1998) Estimation of source parameters and Q from acceleration recorded in the Vatnafjtll earthquake in south Iceland. Bull Sesmic Soc Am 88(2):556–563

Oliveira CS, Lemos JV, Sincraian GE (2002) Modelling large displacements of structures damaged by earthquake motions. European Earthquake Engineering 3:56–71

Reches Z, Dieterich JH (1983) Faulting of rocks in three-dimensional strain fields. I: failure of rocks in poliaxial, servo control experiments. Tectonophysics 95:111–132

Schilling JG (1991) Fluxes and excess temperature of mantle plumes inferred from their interaction with migrating mid-ocean ridges. Nature 352:397–403

Senos ML, Gaspar JL, Cruz J, Ferreira T, Nunes JC, Pacheco JM, Alves P, Queiroz G, Dessai P, Coutinho R, Vales D, Carrilho F (1998) O terramoto do Faial de 9 de Julho de 1998. 1° Simpósio de Meteorologia e Geofísica da APMG Lagos, 61–67

Senos ML, Alves PM, Vales D, Cruz J, Silva M, Carrilho F (2008) Sismo de 9 de Julho de 1998 nos Açores e a crise sísmica associada—dez anos depois, Sismo 1998—Açores. Uma década depois. In Oliveira CS, Costa A, Nunes JC (eds) Governo dos Açores/SPRHI, S.A., 73–87

Spence R (ed) (2007) Earthquake disaster scenario prediction and loss modelling for urban areas. LessLoss Report No 7, ISBN 978-88-6198-011-2, p 165. http://elsa.jrc.ec.europa.eu/events.php?id=4

Spudich P, Xu L (2003) Documentation of software package Compsyn sxv3.11. In International Handbook of Earthquake and Engineering Seismology CD, IASPEI, Academic Press

Vogt PR (1976) Plumes, subaxial pipe-flow, and topography along mid-oceanic ridge. Earth Planet Sci Lett 29(2):309–325

Wald DJ, Quintoriano V, Heaton TH, Kanamori H (1999) Relationships between peak ground acceleration, peak ground velocity, and modified Mercalli intensity in California in California. Earthquake Spectra 15(3):557–564

Watson DF, Philip GM (1985) A refinement of inverse distance weighted interpolation. Geoprocessing 2:315–327

Wells DL, Coppersmith KJ (1994) New empirical relationships among magnitude, rupture length, rupture width, rupture area, and surface displacement. Bull Seism Soc Am 84:974–1002

Yang T, Shen Y, Van der Lee S, Solomon SC, Hung SH (2006) Upper mantle structure beneath the Azores hotspot from finite-frequency seismic tomography. Earth Planet Sci Lett 250:11–26

Zonno G, Rotondi R, Brambilla C (2009) Mining macroseismic fields to estimate the probability distribution of the intensity at site. Bull Seism Soc Am 99(5):2876–2892